Letter

Negative and zero thermal expansion in $K_{0.5}Bi_{0.5}TiO_3$

Gobinda Das Adhikary,[1,2] Pooja Punetha,[1,2] Ram Prakash Singh,[1] Vivek Dwij,[3] Vasant Sathe,[3] Anatoliy Senyshyn,[4] Pavan Nukala,[2] and Rajeev Ranjan[1,*]

[1]*Department of Materials Engineering, Indian Institute of Science, Bangalore-560012, India*
[2]*Center for Nanoscience and Engineering, Indian Institute of Science, Bangalore-560012, India*
[3]*UGC-DAE Consortium for Scientific Research, University Campus, Khandwa Road, Indore 452001, India*
[4]*Forschungsneutronenquelle Heinz Maier-Leibnitz (FRM II), Technische Universität München, Lichtenbergestrasse 1, D-85747 Garching b. München, Germany*

(Received 9 March 2023; accepted 4 October 2023; published 17 October 2023)

We show that a synergy of the covalency effect associated with the *A*-site and *B*-site cations in $K_{0.5}Bi_{0.5}TiO_3$ (KBT) makes it unique among the Pb-free ferroelectrics by imparting a rare property of negative and zero thermal expansion (ZTE). We tuned this synergy in two different KBT alloys, $K_{0.5}Bi_{0.5}TiO_3 - Na_{0.5}Bi_{0.5}TiO_3$ and $K_{0.5}Bi_{0.5}TiO_3 - Bi(Mg_{0.5}Ti_{0.5})O_3$, and identified a common critical tetragonality below which the ZTE behavior disappears completely in both the systems.

DOI: 10.1103/PhysRevB.108.L140104

The anharmonic nature of the interatomic potential renders average solids to exhibit positive thermal expansion (PTE) as per the Debye-Grüneisen relationship [1]. However, on occasions, other factors (structural, magnetic, electrical) may intervene and compete with the PTE tendency to impart nearly zero thermal expansion (ZTE) or even negative thermal expansion (NTE) behavior. The well-known invar effect in the ferromagnetic phase of the Fe-Ni alloy is a case in point wherein the volume expansion caused by magnetostriction nearly compensates for the volume decrease associated with the anharmonic interactions [2,3] when cooled below the magnetic Curie point. Similar behavior has also been reported in $SrRuO_3$ below ∼160 K [4]. In solids with open-framework structures such as ZrW_2O_8, NTE occurs due to the dominant influence of the volume-decreasing structural mode corresponding to the M_1-O-M_2 linkages [5]. In ferroelectric systems, the intrinsic coupling of strain and the polarization degrees of freedom ensures the expansion of the lattice along the polar axis when the spontaneous polarization sets in below the ferroelectric Curie point. However, NTE can be seen only in a narrow temperature range around the Curie point in most ferroelectric systems. In this context, $PbTiO_3$ is unique as it exhibits NTE well below its Curie point, ∼490 °C [6]. To emphasize this point, we compare in Fig. 1 the temperature dependence of unit-cell volume of $BaTiO_3$ (BT) and $PbTiO_3$ (PT). While for PT, the NTE behavior can be seen in the temperature interval 490° C–25 °C, for BT (Curie point 130 C), the NTE behavior is limited in the temperature interval 130 °C–120 °C. The striking difference in the thermal expansion behaviors in BT and PT ferroelectric states lies in the slight difference in chemical interactions driving ferroelectricity. While the *B*-O hybridization is essential for the stability of the ferroelectric state in ABO_3 perovskites in general, the presence of ions with $6s^2$ lone-pair electrons at the *A* site (such as Pb^{+2} and Bi^{+3}) increases the stability of ferroelectric state (high Curie point) as in $PbTiO_3$ (PT) and $BiFeO_3$ (PT) [7,8]. In $PbTiO_3$, the synergy of strong Pb-O hybridization along with the covalent Ti-O interaction stabilizes the tetragonal ferroelectric ground state with a relatively large tetragonality ($c/a-1 = 0.06$) [7]. In contrast, the Ba-O interaction in BT is ionic and does not contribute significantly toward the stability of the ferroelectric state. The ferroelectric ground state of BT is rhombohedral. Despite the strongly covalent Bi-O interaction contributing to the stability of the ferroelectric state in BF, it, too, stabilizes in a rhombohedral ferroelectric ground state. Unlike $PbTiO_3$, BF does not show NTE behavior. However, when alloyed with PT, a synergy of the $6s^2$ lone-pair effect due to Pb^{+2} and Bi^{+3} on the *A* site, together with an increased population of the covalent Ti-O interaction on the *B* site, stabilizes a tetragonal ferroelectric phase with a remarkably large tetragonality ($c/a-1 \sim 0.18$), three times that of PT ($c/a-1 = 0.06$) [6,9]. This tetragonal phase exhibits NTE behavior [6].

Given the crucial role of the synergy that comes into being when the *A* site of the perovskite is sufficiently populated with atoms with $6s^2$ lone-pair electrons and the *B* site with Ti atoms in stabilizing the tetragonal ferroelectric phase exhibiting NTE behavior, a similar scenario can be envisaged in Bi-based Pb-free ferroelectrics. In this context, the ferroelectric compounds $Na_{0.5}Bi_{05}TiO_3$ (NBT) [10] and $K_{0.5}Bi_{0.5}TiO_3$ [11] are worth considering. Among the two, the rhombohedral ground state of NBT [10] makes it analogous to BF, and NTE is not likely to occur. KBT, which exhibits a tetragonal ferroelectric state, appears analogous to $PbTiO_3$ and is the most plausible candidate for showing NTE behavior. In contrast to $PbTiO_3$, wherein the occupancy of atoms containing $6s^2$ lone-pair electron is 100% on the *A* site, the population of Bi^{+3} on the *A* site of KBT is 50%. The lone-pair contribution to the stability of the tetragonal ferroelectric phase is expected to be significantly diluted in KBT. However, the nearly double tetragonality of KBT ($c/a-1 = 0.02$) as compared to $BaTiO_3$

*rajeev@iisc.ac.in

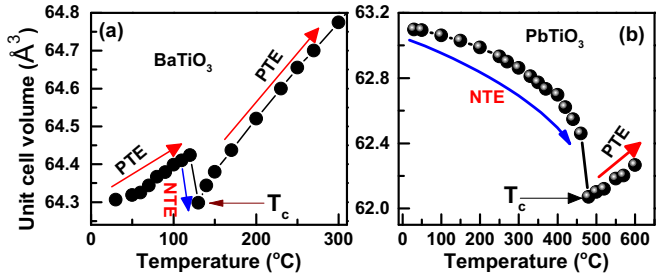

FIG. 1. Temperature dependence of tetragonal unit-cell volume: (a) $BaTiO_3$ and (b) $PbTiO_3$. $T_C \rightarrow$ Curie point; PTE, ZTE, and NTE indicate positive, zero, and negative thermal expansions, respectively.

$(c/a–1 = 0.01)$ indicates that the Bi^{+3} $6s^2$ lone-pair electron contribution is still prominent, and KBT might show NTE behavior. This interesting possibility in KBT, however, has not been explored. Most interest in KBT has so far been limited to the use of its tetragonal ferroelectric phase for the design of morphotropic phase boundary (MPB) compositions by alloying with rhombohedral NBT for enhanced electromechanical response [12–16].

KBT specimens were synthesized using the conventional solid-state reaction method, the details of which can be found in the Supplemental Material [17]. Figure 2(a) shows the temperature dependence of the volume of KBT across the depolarization temperature. It exhibits a positive volume thermal expansion above 350 °C, negative thermal expansion in 300 °C–360 °C range, and nearly zero thermal expansion in a significantly large temperature interval of 100 °C–300 °C. The NTE behavior sets in at ∼300 °C even while the system exhibits a relaxor ferroelectric-like behavior above 300 °C [Figs. S1(b) and S1(c)] [17]. In this temperature regime (280 °C–350 °C), KBT exhibits a tetragonal ($P4mm$) + cubic mixed structural state on the global scale [Fig. S1(a)] [17]. The ZTE and PTE (below 100 °C) behavior is seen in the temperature regime when the cubiclike phase becomes invisible [Fig. S1(a)] [17].

We also investigated the lattice thermal expansion behavior in two different chemically modified variants of KBT, namely (i) $(1-x)$KBT $-$ (x)NBT (in short, KBT $-$ xNBT) and (ii) $(1-y)$KBT $-$ $(y)Bi(Mg_{0.5}Ti_{0.5})O_3$ (in short, KBT $-$ yBMT). The alloy NBT-KBT represents A-site modified KBT (a fraction of K replaced by Na, keeping the population of Bi unchanged). KBT-BMT, on the other hand, has a small fraction of Ti replaced by Mg. In both the systems, the Bi fraction has not been diluted vis-à-vis the parent compound KBT, thereby retaining the contribution of the $6s^2$ lone-pair atoms on the A site in stabilizing the ferroelectric tetragonal phase. Since the primary objective was to tune the synergy between the A-O and B-O interactions that lead to the NTE and ZTE behavior, the concentration of the chemical modifications was limited to those which preserved the tetragonal ferroelectric phase (NTE and ZTE are observed only in this phase). The NTE and ZTE behaviors persist in Na-modified KBT, i.e., $(1-x)$KBT $-$ (x)NBT up to $x = 0.58$ [Fig. 2(b), and Figs. S2(a), 2(b), and S3] [17]. The temperature interval (ΔT) exhibiting the NTE and ZTE, however, decreases with increasing the Na concentration [Fig. 2(e)]. For

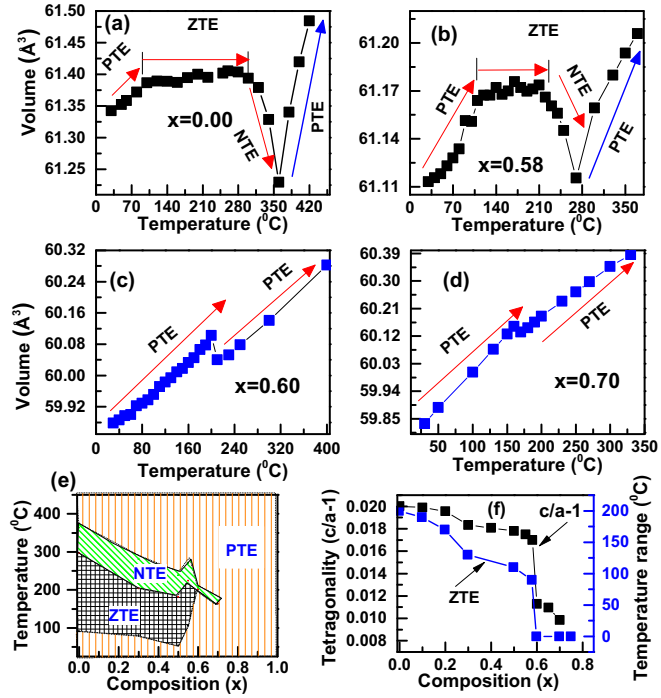

FIG. 2. Temperature evolution of unit-cell volume of tetragonal ($P4mm$) phase in $(1-x)K_{0.5}Bi_{0.5}TiO_3 - (x)Na_{0.5}Bi_{0.5}TiO_3$ [$(1-x)$KBT $-$ (x)NBT]: (a) $x = 0.00$, (b) $x = 0.58$, and (c) $x = 0.60$; PTE, ZTE, and NTE indicate positive, zero, and negative thermal expansions, respectively. (d) Composition dependence of temperature range in which ZTE and NTE occur. Temperature ranges of ZTE and NTE suddenly collapse at $x = 0.60$. Phase diagram of (e) KBT-(x)NBT, which highlights temperature ranges for ZTE, NTE, and PTE. (f) Tetragonality and temperature range in which ZTE occurs as function of composition in KBT-(x)NBT system.

$x = 0.58$, for example, the ZTE can be seen in the temperature range 100 °C–200 °C, i.e., $\Delta T \sim 100$ °C. For unmodified KBT, on the other hand, $\Delta T \sim 200$ °C (100 °C–300 °C). Intriguingly, the ZTE behavior disappears abruptly for $x > 0.58$ [Figs. 2(c), 2(d), and S2(c)] [17]. Figure 2(e) summarizes the thermal expansion behavior of KBT-NBT in the composition-temperature space. Although this abrupt change in the thermal expansion behavior for $x > 0.58$ suggests a qualitative change in the lattice property, x-ray-powder diffraction (XRPD) did not reveal any structural change; the diffraction pattern of $x = 0.58$ (showing NTE and ZTE) is the same as that of $x = 0.60$ (exhibiting no NTE and ZTE) (Fig. S3) [17]. The tetragonality $(c/a - 1)$, however, exhibits an abrupt drop at $x = 0.60$ [Fig. 2(f)], suggesting the onset of a subtle structural order, the signature of which is not identifiable by the XRPD technique. Figures 3(a) and 3(b) shows electron diffraction patterns of two representative compositions, $x = 0.50$ (which shows NTE and ZTE behavior) and $x = 0.60$ (which does not show NTE and ZTE behavior). The 111 zone-axis selected-area diffraction pattern (SADP) of $x = 0.60$ shows $1/2\{ooe\}$ type of superlattice reflections. Similar superlattice spots are also seen in the SADP of the $[\bar{1}30]$ zone axis in Fig. S4(d) [17]. Few grains show faint $1/2\{ooo\}$-type reflections in the pattern corresponding to the [110] zone axis [Fig. S4(b)] [17], suggesting the occasional

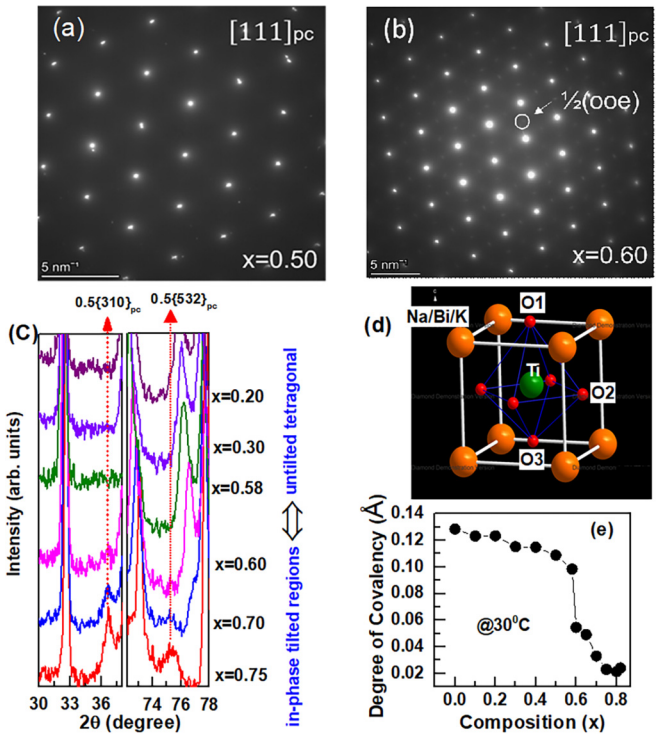

FIG. 3. [111]pc zone-axis electron-diffraction patterns of $(1-x)$KBT $-$ (x)NBT for (a) $x = 0.50$ and (b) $x = 0.60$. (c) Composition evolution of neutron powder-diffraction pattern of $(1-x)$KBT $-$ (x)NBT in two different limited 2θ ranges. Weak superlattice peaks are indicated by red arrows. (d) Schematic diagram of tetragonal unit cell. (e) Composition dependence of difference in lengths of Ti–O_1 and Ti–O_3 bonds at room temperature. This difference is treated as measure of intrinsic polarization. Intrinsic polarization drops abruptly for $x > 0.58$, confirming weakening of polarization by onset of in-phase octahedral tilt.

presence of antiphase octahedral tilt (corresponding to the rhombohedral $R3c$ structure) on the local scale. In contrast, no superlattice spots were observed in the SADP patterns of $x = 0.50$ [Fig. 3(b), and Figs. S4(a) and S4(c)] [17]. These observations indicate a correlation between the octahedral tilt and the disappearance of the ZTE behavior in this system.

Figure 3(c) shows a vertically magnified NPD pattern of $(1-x)$KBT $-$ (x)NBT for different compositions in a limited 2θ range. The full diffraction pattern is shown in Fig. S5 [17]. Consistent with the SADP, the NPD patterns also exhibit weak superlattice reflections of type $1/2\{ooe\}$ for $x \geqslant 0.60$ [Fig. 3(c)]. For NBT-based ferroelectrics such superlattice reflections are generally associated with the $P4bm$ phase [12,18]. However, as shown in Fig. S6(b) [17], this structural model is inadequate to precisely account for the intensity of the superlattice peaks. As argued in another publication [18], this is most likely due to the absence of a long range of the in-phase octahedral tilt. If we ignore these weak superlattice peaks, the fundamental Bragg profiles can be nicely accounted for with the $P4mm$ ferroelectric tetragonal structural model [Fig. S6(a)] [17]. We therefore persisted with the strategy of fitting the neutron powder-diffraction patterns of all the tetragonal compositions with the $P4mm$ structural model [Figs. S7(a)–S7(c)] [17] and extracted the atomic parameters and bond distances as a function of compositions (for all $x < 0.80$). Due to the large isotropic displacement parameters (>4 Å^2) of the A-site cations (Na/K/Bi), we instead refined the anisotropic displacement parameters of these atoms (Table S1 and Table S2) [17]. Only the isotropic displacement parameters were refined for the remaining atoms to minimize the number of independent parameters. The refinement was performed in a sequential manner; the best-fit parameters obtained for a given composition were fed as the initial input parameter of the adjacent composition of the series.

In tetragonal ferroelectrics wherein the covalency associated with the A-O interaction plays an important role in stabilizing the tetragonal ground state (as in $PbTiO_3$ and $BiFeO_3 - PbTiO_3$ systems), the tetragonality and the polarization are known to be notably large compared to the case (like $BaTiO_3$) where the A-site atoms do not contribute to the stability of the ferroelectric state. One good measure of the prevalent synergy between the covalency effects associated with the A-site and B-site cations in tetragonal ferroelectric perovskite is the difference in the Ti–O_1 and Ti–O_3 bonds parallel to the c axis [19] [Fig. 3(d)]. As shown in Fig. 3(e), the abrupt decrease of this parameter on increasing the Na content from $x = 0.58$ to $x = 0.60$ is consistent with the abrupt decrease in the degree of the synergy between the A- and

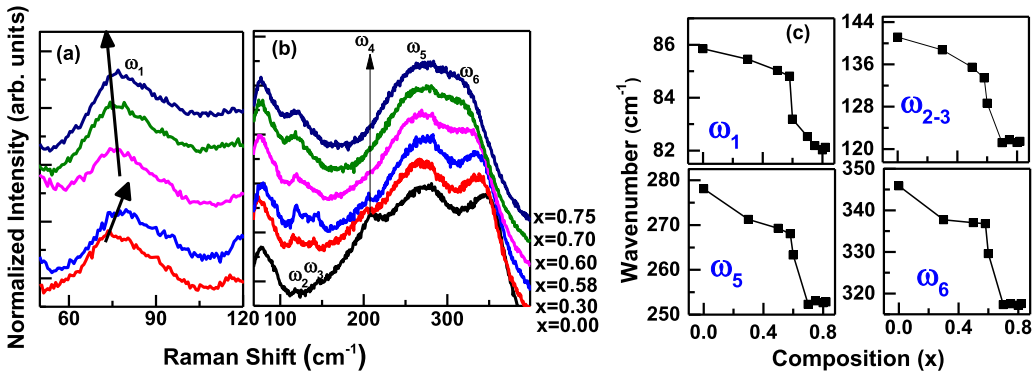

FIG. 4. (a), (b) Raman spectra of representative compositions in their ferroelectric state at room temperature. Arrows highlight abrupt change in nature of peak shift for $x > 0.58$. (c) Composition dependence of frequencies of different modes at 30 °C. Frequencies of modes ω_1 corresponding to Na/Bi/K-O vibration, ω_{2-3} $(= [(\omega_2^2 + \omega_3^2)/2]^{1/2})$ related to coupling of off-centered Na/Bi/K and off-centered Ti cations, and ω_4, ω_5, ω_6 corresponding to Ti-O vibrations decrease suddenly at $x = 0.60$ at room temperature.

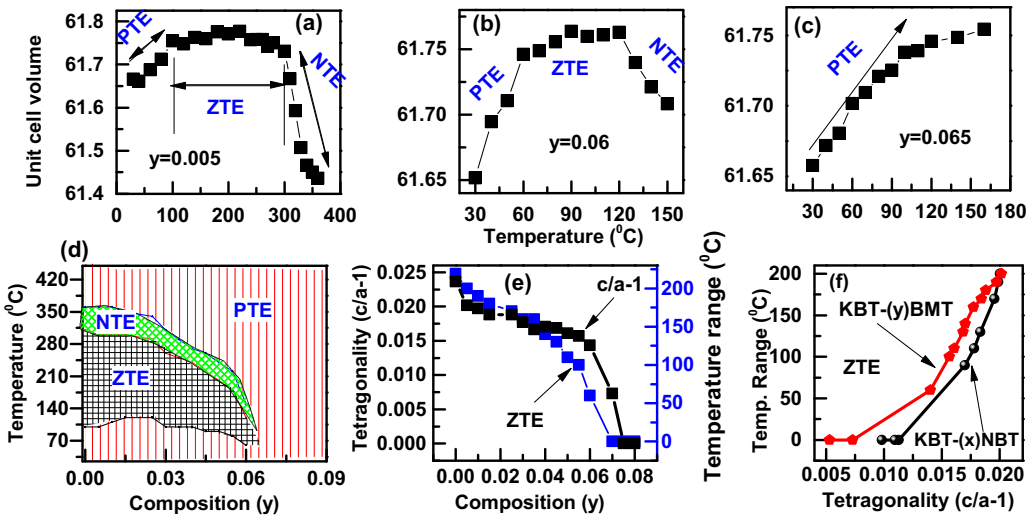

FIG. 5. Temperature evolution of unit-cell volume of tetragonal ($P4mm$) phase in $(1-y)K_{0.5}Bi_{0.5}TiO_3-(y)Bi(Mg_{0.5}Ti_{0.5})TiO_3$ [$(1-y)$KBT $-$ (y)BMT]: (a) $y = 0.005$, (b) $y = 0.06$, and (c) $y = 0.065$. (d) Composition-temperature diagram highlighting temperature ranges for ZTE, NTE, and PTE. (e) Composition dependence of tetragonality and temperature range for ZTE. (f) Comparison of tetragonality dependence of temperature range of ZTE of KBT-(x)NBT and KBT-(y)BMT systems.

B-site cations stabilizing the tetragonal ferroelectric phase. The disappearance of the NTE/ZTE properties for $x > 0.58$ in KBT-NBT can be attributed to the weakening of this synergy by the onset of the in-phase octahedral tilt.

The abrupt change for $x > 0.58$ was also captured in the phonon (Raman) spectra of this system (Fig. 4). The spectra were fitted with Lorentzian profiles after correcting for the Bose-Einstein occupation factor [Figs. S8(a) and S8(b) and Figs. S9(a) and S9(b)] [17]. Of the 15 Raman-active modes ($\Gamma_{\text{Raman, KBT}} = 3A_1 + 3B_1 + 2B_2 + 7E$ [20]) anticipated for the tetragonal ($P4mm$) structure of KBT, 11 first-order Raman active modes were observed [Fig. S8(a)] [17]. The Raman spectrum of perovskites can be categorized into four regions [21]: (1) 30–90 cm^{-1}, which primarily involves A-site cations and is therefore sensitive to A-site off centering; (2) the $A-BO_3$ modes in the range 100–180 cm^{-1} are associated with dynamic coupling of the off-centered A-site and off-centered B-site cations; (3) B-cation vibration modes in the range of 220–400 cm^{-1}; and (4) modes corresponding to tilting of the BO_6 octahedra in the range of 420–650 cm^{-1}. A careful observation of the Raman spectra revealed the following distinct features : (i) The frequency of low-energy phonon mode (ω_1) involving Na/Bi/K cation vibrations around 60–80 cm^{-1} decreases abruptly at $x = 0.60$ [Fig. 4(c)]; (ii) the peaks of the two modes $\omega_2 \sim 120\,cm^{-1}$ and $\omega_3 \sim 146\,cm^{-1}$ are much more prominent for the compositions $x \leqslant 0.58$; (iii) the mode ω_3 weakens abruptly at $x = 0.60$; and (iv) the mode $\omega_4 \sim 208\,cm^{-1}$ involving Ti cation displacement also disappears around the same composition, $x = 0.60$. The distinct drop in the frequencies of the ω_1, ω_{2-3}, ω_5, and ω_6 at $x = 0.60$ [Fig. 4(c)] suggests a flattening of A-site and B-site potential barriers [21,22], consistent with the abrupt drop in the tetragonality.

We attempted to tune the covalency effect in another system, $(1-y)$KBT $-$ $(y)Bi(Mg_{0.5}Ti_{0.5})O_3$, by replacing a small fraction of the Ti on the B site with Mg (a nonferroelectric active element). The absence of superlattice peaks in the NPD patterns (Fig. S10 and Fig. S11) [17] of this series confirmed the absence of octahedral tilt [23]. Lattice thermal expansion measurements performed on this series [Figs. 5(a)–5(c), and Fig. S12] [17] revealed the persistence of ZTE up to $y = 0.06$. The ZTE behavior disappeared at $y = 0.065$ [Figs. 5(c) and 5(d)]. Similar to the KBT-NBT, a one-to-one correlation between the tetragonality $(c/a-1)$ and the temperature range of ZTE behavior can be seen. The ZTE vanishes when the tetragonality decreases below 1.4% [Fig. 5(f)]. Interestingly, this critical tetragonality is the same as the critical tetragonality below which ZTE disappears in KBT-NBT [Fig. 5(f)]. This implies that the tetragonality of 1.4% is an indicator of the threshold value for the system to exhibit the NTE/ZTE behavior. That this critical value is higher than the tetragonality of $BaTiO_3$ (1%) is consistent with the fact that $BaTiO_3$ does not show ZTE behavior (Fig. 1).

In summary, we show that $K_{0.5}Bi_{0.5}TiO_3$ is unique among the Pb-free ferroelectric compounds wherein the synergy between the A-site and B-site cations helps stabilize a tetragonal ferroelectric phase which exhibits a rare phenomenon of zero thermal expansion over a large temperature interval. We investigated this phenomenon in two different KBT alloy systems and identified a critical tetragonality ($c/a-1 \sim 1.4\%$) indicative of the persistence of this synergy effect. The understanding developed here can be useful in designing ZTE materials at room temperature for practical applications.

R.R. acknowledges Science and Engineering Research Board for financial assistance (Grant No. CRG/2021/000134). Part of this work was carried out at the Micro and Nano Characterization Facility (MNCF) located at CeNSE, IISc Bengaluru, funded by NPMAS-DRDO and MCIT, MeitY,

Government of India, and benefited from all the help and support from the staff. P.N. and P.P. also would like to thank Advanced Facility for Microscopy and Microanalysis (AFMM), IISc.

[1] E. Grüneisen, Theory of the solid state of monatomic elements, Ann. Phys. **39**, 257 (1912); Handb. Phys. **10**, 1 (1926).

[2] C. E. Guillaume, Research on nickel steels, C. R. Acad. Sci. **125**, 235 (1897).

[3] P. Mohn, A century of zero expansion, Nature (London) **400**, 18 (1999).

[4] T. Kiyama, K. Yoshimura, K. Kosuge, Y. Ikeda, and Y. Bando, Invar effect of $SrRuO_3$: Itinerant electron magnetism of Ru 4*d* electrons, Phys. Rev. B **54**, R756(R) (1996).

[5] T. A. Mary, J. S. O. Evans, T. Vogt, and A. W. Sleight, Negative thermal expansion from 0.3 to 1050 Kelvin in ZrW_2O_8, Science **272**, 90 (1996).

[6] J. Chen, L. Hu, J. Deng, and X. Xing, Negative thermal expansion in functional materials: Controllable thermal expansion by chemical modifications, Chem. Soc. Rev. **44**, 3522 (2015).

[7] R. E. Cohen, Origin of ferroelectricity in perovskite oxides, Nature (London) **358**, 136 (1992).

[8] J. B. Neaton, C. Ederer, U. V. Waghmare, N. A. Spaldin, and K. M. Rabe, First-principles study of spontaneous polarization in multiferroic $BiFeO_3$, Phys. Rev. B **71**, 014113 (2005).

[9] B. Narayan, Y. A. Sorb, B. Loukya, A. Samanta, A. Senyshyn, R. Datta, A. K. Singh, C. Narayana, and R. Ranjan, Interferroelectric transition as another manifestation of intrinsic size effect in ferroelectrics, Phys. Rev. B **94**, 104104 (2016).

[10] G. A. Smolenskii, V. A. Isupov, A. I. Agranovskaya, and N. N. Krainik, New ferroelectrics of complex composition, Sov. Phys. Solid State **2**, 2651 (1961).

[11] G. A. Smolenskii, Dielectric polarization of a series of compounds of complex composition, Sov. Phys. Solid State **1**, 1562 (1959).

[12] M. Otonicar, S. D. Škapin, and B. Jancar, TEM analyses of the local crystal and domain structures in $(Na_{1-x}K_x)_{0.5}Bi_{0.5}TiO_3$ perovskite ceramics, IEEE Trans. Ultrason. Ferroelectr. Freq. Control **58**, 1928 (2011).

[13] T. Takenaka, H. Nagata, and Y. Hiruma, Phase transition temperatures and piezoelectric properties of $(Bi_{1/2}Na_{1/2})TiO_3$-and $(Bi_{1/2}K_{1/2})TiO_3$-based bismuth perovskite lead-free ferroelectric ceramics, IEEE Trans. Ultrason. Ferroelectr. Freq. Control **56**, 1595 (2009).

[14] G. D. Adhikary, D. K. Khatua, A. Senyshyn, and R. Ranjan, Random lattice strain and its relaxation towards the morphotropic-phase-boundary of $Na_{0.5}Bi_{0.5}TiO_3$-based piezoelectrics: Impact on the structural and ferroelectric properties, Phys. Rev. B **99**, 174112 (2019).

[15] A. Sasaki, T. Chiba, Y. Mamiya1, and E. Otsuki, Dielectric and piezoelectric properties of $(Bi_{0.5}Na_{0.5})TiO_3$–$(Bi_{0.5}K_{0.5})TiO_3$ systems, Jpn. J. Appl. Phys. **38**, 5564 (1999).

[16] G. D. Adhikary, D. K. Khatua, A. Senyshyn, and R. Ranjan, Long-period structural modulation on the global length scale as the characteristic feature of the morphotropic phase boundaries in the $Na_{0.5}Bi_{0.5}TiO_3$ based lead-free piezoelectrics, Acta Mater. **164**, 749 (2019).

[17] See Supplemental Material at http://link.aps.org/supplemental/10.1103/PhysRevB.108.L140104 for (i) specimen preparation and characterization, (ii) high-temperature NPD and XRPD patterns and Rietveld refinements of these patterns, and (iii) Raman spectroscopy and TEM data.

[18] G. D. Adhikary, B. Mahale, B. N. Rao, A. Senyshyn, and R. Ranjan, Depoling phenomena in $Na_{0.5}Bi_{0.5}TiO_3 - BaTiO_3$: A structural perspective, Phys. Rev. B **103**, 184106 (2021).

[19] V. Kothai, A. Senyshyn, and R. Ranjan, Competing structural phase transition scenarios in the giant tetragonality ferroelectric $BiFeO_3 - PbTiO_3$: Isostructural vs multiphase transition, J. Appl. Phys. **113**, 084102 (2013).

[20] J. Kreisel, A. M. Glazer, G. Jones, P. A. Thomas, L. Abello, and G. Lucazeau, An x-ray diffraction and Raman spectroscopy investigation of A-site substituted perovskite compounds: The $(Na_{1-x}K_x)_{0.5}Bi_{0.5}TiO_3$ $(0 \leqslant x \leqslant 1)$ solid solution, J. Phys.: Condens. Matter **12**, 3267 (2000).

[21] K. Datta, R. B. Neder, A. Richter, M. Göbbels, J. C. Neuefeind, and B. Mihailova, Adaptive strain prompting a pseudo-morphotropic phase boundary in ferroelectric $(1-x)Na_{0.5}Bi_{0.5}TiO_3 - xBaTiO_3$, Phys. Rev. B **97**, 184101 (2018).

[22] K. Datta, A. Richter, M. Gobbels, R. B. Neder, and B. Mihailova, Atomistic origin of huge response functions at the morphotropic phase boundary of $(1-x)Na_{0.5}Bi_{0.5}TiO_3 - xBaTiO_3$, Phys. Rev. B **90**, 064112 (2014).

[23] A. Zeb, D. A. Hall, Z. Aslam, J. Forrester, J. F. Li, Y. Li, C. C. Tang, G. Wang, F. Zhu, and S. J. Milne, Structure-property relationships in the lead-free piezoceramic system $K_{0.5}Bi_{0.5}TiO_3 - BiMg_{0.5}Ti_{0.5}O_3$, Acta Mater. **168**, 100 (2019).